# Physico–chemical Modelling of Adlayer Phase Formation via Surface–limited Reactions of Copper in Relation to Sequential Electrodeposition of Multilayered Platinum on Crystalline Gold

**Tumaini S. Mkwizu** [a,*] **and Ignacy Cukrowski** [a,*]

[a] Department of Chemistry, University of Pretoria, Hatfield, Lynnwood Road, Pretoria, 0002, South Africa

* Corresponding authors' address: Department of Chemistry, University of Pretoria, Hatfield, Lynnwood Road, Pretoria, 0002, South Africa.

Tel: +27 12 420 3988; fax: +27 12 420 4687.

E–mail: tumaini.mkwizu@tuks.co.za (T.S.M); ignacy.cukrowski@up.ac.za (I. C.)

**ACCEPTED AUTHOR MANUSCRIPT (POST-PRINT)****

****NOTICE: this is the author's version of a work that was accepted for publication in Electrochimica Acta. Changes resulting from the publishing process, such as peer review, editing, corrections, structural formatting, and other quality control mechanisms may not be reflected in this document. Changes may have been made to this work since it was submitted for publication. A definitive version was subsequently published in ELECTROCHIMICA ACTA, VOL. 147 (2014) pp. 432-441 DOI: 10.1016/j.electacta.2014.09.086**

# ABSTRACT

Electrochemical physico-chemical models, describing isothermically surface coverage dependency with electrode potential of underpotentially deposited Cu adlayers ($Cu_{UPD}$) as well as successive surface-limited redox replacement (SLRR) reactions between $Cu_{UPD}$ and $PtCl_6^{2-}$, to form multilayered Pt deposits on crystalline Au, have been explored. Modelling of such phase formation phenomena take into account heterogeneity effects and extent of adatom interactions within the adlayers on the base Au substrate and gradually formed Pt multilayered deposits. Insights on exchanged electrons, phenomenological reaction kinetics and Gibbs free energy variations during various deposition stages involving SLRR reactions are divulged.

**KEYWORDS**

Underpotential deposition

Surface–Limited Redox–Replacement

Multilayered Platinum Nanostructures

Adsorption Isotherms

Kinetics

## 1. INTRODUCTION

Electrochemical deposition of transition metals, with atomic control using single–step or multi–step surface–limited redox–replacement (SLRR) reactions, is of fundamental and potential technological importance in fabrication of monolayer–decorated nanoparticles, monolayer–coated surfaces, epitaxial ultra–thin films, as well as multilayered nanoclusters [1-14]. In a typical SLRR reaction (Reaction (1)), an adlayer of a metal *M* formed electrochemically through underpotential deposition (UPD) [15, 16] on a substrate *S* ($M_{UPD}$/S; Reaction (2)), is spontaneously re–oxidized by open–circuit (OC) contact with ions $N^{p+}$ of a more noble metal *N*; the overall process culminates in formation of an adlayer of metal *N* on *S* [1, 12].

$$M_{UPD}/S + (z/p)\, N^{p+} \leftrightarrow M^{z+} + (z/p)\, N/S \quad (1)$$

$$(M^{z+} + ze^{-})/S \rightarrow M_{UPD}/S \quad (2)$$

The development of formalisms to understand thermodynamic and kinetic factors governing such SLRR reactions can be regarded as being at their infancy. Since phase formation by SLRR reaction is intimately linked to UPD (both processes being surface-limited in their overall outcome), formalisms thus far explored are derived from well–established physico–chemical models of UPD; a phenomenon that has been extensively explored in electrochemical literature prior to exploration of the SLRR deposition methodology [12, 17]. The realization that thermodynamically the chemical potential of a metal in a monolayer could be lower than its chemical potential in the bulk metal, hence, its activity in a monolayer can be less than unity, have led to various UPD models based on phase transitions or specific adsorption formalisms

aimed at describing the potential–dependence or charge–dependence of surface coverage of UPD adlayers [15, 18-23].

In particular, UPD has been modelled through formalisms based on the so-called 'pseudo–Nernstian' relationships between the electrode potential and surface activity of formed adlayer where the standard state can be phenomenologically chosen to correspond to the bulk metal or an appropriate submonolayer state [19-21, 24-26]. To this effect, the surface coverage phenomena resulting from UPD process are describable through electrochemical adsorption isotherms. Modelling of the UPD processes based on Langmuir–type isotherm presumes adlayer formation on a homogeneous surface and neglects any interactions between the adatoms within the adlayer. More involved models, such as those derived from Temkin and Frumkin isotherms, take into account surface heterogeneity, adatom–substrate interactions, adatom–adatom interactions as well as induced surface effects upon adlayer adsorption/desorption [24, 25, 27-29]. Moreover, the relationship between surface coverage of adlayers generated by UPD ($\theta_{\mathrm{UPD}}$) and the activity of the depositing species in the coverage range $0 \leq \theta_{\mathrm{UPD}} \leq 1$, may be approximated in terms of a thermodynamic formalism based on the concept of "submonolayer equilibrium potential" [25], formulated within the framework of equal electrochemical potentials of the parent species in solution and in the corresponding substrate phases. Effectively, the submonolayer equilibrium potential during a UPD process (Reaction (2)) can be defined as

$$E_{\mathrm{UPD}} = E^{\mathrm{o}}_{\mathrm{UPD}} + \frac{RT}{zF} \ln \frac{a_{\mathrm{M}^{z+}}}{a_{\mathrm{M,UPD}}} \tag{3}$$

where $R$, $T$, $z$ and $F$ have their usual meaning; $a_{\mathrm{M,UPD}}$ is the activity of adlayer of metal $M$ at coverage $\theta_{\mathrm{UPD}}$ (the latter is described by an appropriate potential–coverage isotherm); $E^{\mathrm{o}}_{\mathrm{UPD}}$ is

the standard submonolayer potential which is related to the standard Gibbs free energy of the underlying UPD process by $\Delta G^{\circ}_{\mathrm{UPD}} = -zFE^{\circ}_{\mathrm{UPD}}$. Considering the Langmuir-type isotherm, $E_{\mathrm{UPD}}$ dependence on the submonolayer coverage can be described by Eq. (4) [25, 26]:

$$E_{\mathrm{UPD}} = E^{\theta=0.5} - \frac{RT}{zF}\left[\ln\left(\frac{\theta_{\mathrm{UPD}}}{1-\theta_{\mathrm{UPD}}}\right)\right] \tag{4}$$

where $E^{\theta=0.5}$ corresponds to the potential of surface coverage of 0.5 at unit solution activity.

More complex processes can be modeled through a combined Temkin–Frumkin–type electrochemical isotherm given by Eq. (5) [25-27]:

$$E_{\mathrm{UPD}} = E^{\theta\to 0} - \frac{RT}{zF}\left[\ln\left(\frac{\theta_{UPD}}{1-\theta_{UPD}}\right) + f\theta_{UPD} + g\theta_{UPD}^{3/2}\right] \tag{5}$$

where the parameter $E^{\theta\to 0}$ represents the potential where UPD monolayer formation approaches zero–coverage at unit solution activity; $f$ is an interaction parameter which accounts for (i) heterogeneity effects, (ii) induced work-function changes accompanying surface adlayer formation, and (iii) adatom–substrate interactions; $g$ is an interaction parameter which accounts for lateral adatom–adatom interactions (of electrostatic dipole–dipole nature) that may arise due to charge polarization between the adatoms [25, 27]. Additionally, the $f$ and $g$ parameters largely determine the change of the Gibbs free energy of adlayer formation ($\Delta G_{\mathrm{UPD}}$) with coverage $\theta_{\mathrm{UPD}}$ which can be approximated by Eq. (6):

$$\Delta G_{\mathrm{UPD}} = \Delta G^{\theta\to 0} + RTf\theta_{\mathrm{UPD}} + RTg\theta_{\mathrm{UPD}}^{3/2} \tag{6}$$

where $\Delta G^{\theta\to 0} = -zFE^{\theta\to 0}$.

Focusing on SLRR (Reaction (1)) involving phase formation of an adlayer of the more noble metal *N*, its rate, $r_{\mathrm{SLRR}}$, given by Eq. (7), can be described as either a time-dependent incremental change of surface concentration of the UPD metal adlayer ($C_{\mathrm{M,UPD}}$) or the change in the surface coverage $\theta_{\mathrm{M,UPD}} = \Gamma_{\mathrm{i,UPD}}/C_{\mathrm{M,UPD,}}$ where $\Gamma_{\mathrm{i,UPD}}$ is the initial surface concentration at $t = 0$) [12]. By linking Eq. (5) with appropriate rate equations resulting from Eq. (7), potential-coverage-time models (Eqs. (8) – (10))[12] can be derived. Relevant potential-coverage-time relationships were tacitly demonstrated to be useful for describing phenomenological reaction kinetics and phase formation properties of a single–step SLRR reaction to form a monolayer Pt system on single-crystal Au(111) substrate [12]:

$$r_{\mathrm{SLRR}} = -\frac{\mathrm{d}C_{\mathrm{M,UPD}}}{\mathrm{d}t} = -\Gamma_{\mathrm{i,UPD}}\frac{\mathrm{d}\theta_{\mathrm{M,UPD}}}{\mathrm{d}t} \tag{7}$$

$$E_{\mathrm{SLRR}} = E^{\theta\to 0} - \frac{RT}{zF}\left[\ln\left(\frac{1-k_{\mathrm{o}}t}{k_{\mathrm{o}}t}\right) + f\left(1-k_{\mathrm{o}}\mathrm{t}\right) + g\left(1-k_{\mathrm{o}}\mathrm{t}\right)^{3/2}\right] \tag{8}$$

$$E_{\mathrm{SLRR}} = E^{\theta\to 0} - \frac{RT}{zF}\left[-\left(k_{\mathrm{r1}}t + \ln\left(1-\exp\left(-k_{\mathrm{r1}}t\right)\right)\right) + f\left(\exp\left(-k_{\mathrm{r1}}t\right)\right) + g\left(\exp\left(-k_{\mathrm{r1}}t\right)\right)^{3/2}\right] \tag{9}$$

$$E_{\mathrm{SLRR}} = E^{\theta\to 0} - \frac{RT}{zF}\left[\ln\left(\frac{\left(1+k_{\mathrm{r}}t\right)^{1/(1-N_{\mathrm{or}})}}{1-\left(1+k_{\mathrm{r}}t\right)^{1/(1-N_{\mathrm{or}})}}\right) + f\left(1+k_{\mathrm{r}}t\right)^{1/(1-N_{\mathrm{or}})} + g\left(1+k_{\mathrm{r}}t\right)^{3/(2-2N_{\mathrm{or}})}\right] \tag{10}$$

where $E^{\theta\to 0}$, $f$, $g$, $R$, $T$, $z$, and $F$ have their usual meaning; $N_{\mathrm{or}}$ is the order of the reaction with respect to $M_{\mathrm{UPD}}$ adlayer; and $E_{\mathrm{SLRR}}$ is an open-circuit potential during adlayer formation through an SLRR reaction. $k_0$ in Eq. (8) is a rate constant resulting from the limiting case involving transport-limited redox-replacement of UPD adlayers and a zero-order reaction mechanism ($N_{\mathrm{or}} = 0$). In the case where a diffusional transport of noble metal ions $N^{p+}$ to the substrate's surface

does not limit reaction kinetics, Eqs. (9) – (10) apply. In particular, Eq. (9) is applicable for a first-order reaction mechanism with respect to $M_{\mathrm{UPD}}$ and the phenomenological rate constant $k_{\mathrm{r1}} = k\left(C^{\mathrm{s}}_{\mathrm{N}^{\mathrm{p+}}}\right)^{J_{\mathrm{or}}}\left(\Gamma_{\mathrm{i,UPD}}\right)^{N_{\mathrm{or}}-1}$ where $J_{\mathrm{or}}$ stands for the order of reaction with respect to noble metal ions $N^{\mathrm{p+}}$; $k$ is the fundamental rate constant of the SLRR reaction; and $C^{\mathrm{s}}_{\mathrm{N}^{\mathrm{p+}}}$ is the surface concentration of $N^{\mathrm{p+}}$ ions. Eq. (10) applies for $N_{\mathrm{or}} \neq 0$ and $N_{\mathrm{or}} \neq 1$; the phenomenological rate constant $k_{\mathrm{r}} = k\left(C^{\mathrm{s}}_{\mathrm{N}^{\mathrm{p+}}}\right)^{J_{\mathrm{or}}}\left(\Gamma_{\mathrm{i,UPD}}\right)^{N_{\mathrm{or}}-1}\left(N_{\mathrm{or}}-1\right)$ [12].

It is important to realize that the above formalisms have so far been used to characterize kinetics of phase formation of Pt-monolayer via a single-step UPD/SLRR deposition cycle on single-crystalline Au(111) substrate [12]. Kinetic and thermodynamic phase formation properties following multi-step UPD/SLRR deposition cycles to form noble metallic multilayers have thus far not been studied. Therefore, this work embarked on such systematic investigation of phase formation involving, as a model system, repetitive SLRR reactions between $\mathrm{Cu_{UPD}}$ and $\mathrm{PtCl_6^{2-}}$ complex ion (Reaction (11)).

$$\mathrm{Cu_{UPD}/S} + (z/4)\mathrm{PtCl_6^{2-}} \leftrightarrow \mathrm{Cu^{z+}} + (z/4)\mathrm{Pt/S} + (3z/2)\,\mathrm{Cl^-} \qquad (11)$$

Furthermore, the paper explores the interplay of substrate heterogeneity effects, mass-transport, phase formation kinetics and thermodynamics of SLRR reactions as implemented through successive deposition cycles of Reaction (11) carried out *in situ*. By implication, the substrate *S* is initially a crystalline Au film ($\mathrm{Au_{film}}$) and upon successive deposition cycles it is gradually changed to a layered Pt system. The findings reported herein underpin applicability and generality of submonolayer potential formalism to probe SLRR phase formation processes,

whereby not only electrodic monolayered Pt, but also sequentially-generated multilayered Pt nanostructures are involved.

## 2. EXPERIMENTAL SECTION

### *2.1. Materials*

All solutions were prepared with high–purity deionised water obtained from a Milli–Q water purifier (Millipore Inc. USA) operated at resistivity of about 18 MΩ·cm. All electrochemical experiments were performed in air–conditioned laboratory environment of about 25 °C. 1 x $10^{-3}$ mol/L aqueous precursor electrolyte solutions of $PtCl_6^{2-}$ and $Cu^{2+}$ were made in 0.1 mol/L $HClO_4$; they were prepared from analytical grade $H_2PtCl_6$, $CuSO_4$ reagents and ultra–pure concentrated $HClO_4$ supplied by SA Precious Metals (Pty) and Merck, respectively. The 0.1 mol/L $HClO_4$ solution, at pH 1 ± 0.05, was used as the background electrolyte (BE) solution.

### *2.2. Instrumentation*

A custom–built automated instrumental setup described previously [9] was used for all electrochemical deposition experiments. The setup consisted of piston pumps with electrolyte reservoirs in digitally–controlled exchange units (765 Dosimat, Metrohm), the PGSTAT30 electrochemical workstation operated in potentiostatic mode and a three–electrode flow–cell (Figure 1A) utilising a Ag/AgCl/3M KCl reference electrode (model 6.0727.000, Metrohm Autolab); unless otherwise stated, potentials are reported versus this reference electrode. Electrochemical experiments involving Anodic Stripping Voltammetry (ASV) and Cyclic Voltammetry (CV) were performed with a model PGSTAT30 electrochemical workstation utilising the software packages GPES 4.9 and NOVA 1.6 (Metrohm Autolab, The Netherlands).

*2.3. Electrochemical deposition*

Electrochemical deposition of multilayered Pt on $Au_{film}$ – denoted as $_n(Pt)_{Cu}/Au_{film}$ – proceeded by repetition of *n* deposition cycles schematically shown in Figure 1B–C. Each single cycle involved three stages: (i) rinsing with the BE solution and injection of the sacrificial metal electrolyte, 1 x $10^{-3}$ mol/L $Cu^{2+}$, (ii) deposition of Cu adlayers at UPD followed by BE rinsing, and (iii) OC stage involving injection of 1 x $10^{-3}$ mol/L $PtCl_6^{2-}$ electrolyte solution and SLRR reaction in quiescent conditions. Injection of electrolyte solutions was carried out at flow–rate of 5 mL/min throughout all deposition cycles. Current–time (*i–t*) and potential–time (*E–t*) transients were simultaneously captured *in situ* during the various deposition stages at intervals of 0.2 s. Between the various measurements, the electrochemical cell was rinsed with the BE solution at OC.

*2.4. Physical characterization of the gold substrate*

The deposition substrate was a piece of 300 nm vapour–deposited Au thin–film ($Au_{film}$) coated on a glass slide (with a Ti adhesion layer) as per preparation procedures reported elsewhere [30]. Field Emission Gun Scanning Electron Microscopy (FEG–SEM) was used for *ex situ* analysis of unmodified $Au_{film}$ substrate using model ULTRA PLUS microscope with in–lens capabilities (CARL ZEISS, Germany) operated at 0.5 – 1 kV. X–ray Diffraction (XRD) analysis of the $Au_{film}$ was performed with a model X'Pert PRO powder diffractometer (PANalytical B.V. The Netherlands) equipped with an X'Celerator detector with variable divergence and receiving slits utilizing iron–filtered cobalt–$K_\alpha$ radiation; the phases were identified using X'Pert Highscore plus software. The morphology of the substrate $Au_{film}$ is shown by FEG–SEM micrograph in Figure 2A; clear Au crystallites with distinct grain boundaries are visible. The XRD pattern

(Figure 2B) confirmed that the substrate had somewhat polycrystalline characteristics with prominent composition of (111)–oriented crystallites.

*2.5. Electrochemical characterization*

Prior to flow–cell assembly for electrochemical deposition, the substrate $Au_{film}$ was cleaned in concentrated $HNO_3$ by immersion for 120 s, rinsed with ultra–pure deionized water and, upon assembly in the flow–cell filled with nitrogen–saturated BE solution, by electrochemical cycling between –0.2 V and +1.6 V. The corresponding surface electrochemical behaviour of $Au_{film}$ substrate is exhibited in representative cyclic voltammograms (CVs) shown in Figure 2C. The voltammetric signatures were consistent with surface electrochemistry of a polycrystalline Au electrode in acidic medium in the potential window +0.5 V to +1.6 V where surface Au is transformed from oxidation state of 0 to +3 [31, 32].

The CVs of bare $Au_{film}$ were obtained with maximum anodic potentials between +1.4 V and +1.6 V at various scan rates as shown in Figure 2C. Chronocoulometric analysis of the surface oxide reduction peak (Peak ***a***; Figure 2C), upon scanning to +1.4 V, was consistent with surface adlayer coverage of about 1:1 oxygen–gold structure obtainable below this potential in accordance with known surface electrochemistry of Au electrodes (Reaction (12)) [26, 32-34].

$$x\mathrm{Au} + (x + x/2)\mathrm{H_2O} \leftrightarrow \mathrm{Au}_x\mathrm{O}_{(x+x/2)} + 3x\mathrm{H}^+ + 3x\mathrm{e}^- \qquad (12)$$

Considering the surface oxide generated on the pristine $Au_{film,}$ a nominal charge of 400 $\mu C/cm^2$ was taken as the conversion factor corresponding to the charge required for full 1:1 monolayer (*ML*) coverage [15, 26, 35, 36]; the electrochemical surface area (*ESA*) of the $Au_{film}$ in the flow-cell assembly was thus deduced from conversion of total charge obtained from integration of

Peak ***a*** (Figure 2C)**.** The *ML*–equivalent coverage of Cu on $Au_{film}$ was derived from the total charge of the Cu UPD process ($Q_{UPD}$), obtainable from integration of anodic stripping peaks, taking the area of the electrode as the *ESA*.

Surface coverage of $Cu_{UPD}/Au_{film}$ was probed utilizing ASV at deposition potential ($E_{dep}$) of +0.05 V for variable deposition time ($t_{dep}$). Surface coverage of Cu, as generated by UPD ($\theta_{Cu,UPD}$) on $Au_{film}$, was estimated by numerical integration using Eq. (13) from the corresponding stripping voltammetric data.

$$\theta_{Cu,UPD} = \frac{Q_{Cu,str}}{Q_{Cu,max}} = \frac{\int_{t_j}^{t_q} i\,dt}{Q_{Cu,max}} = \frac{\frac{1}{v}\int_{(E_j-E_0)/v}^{(E_q-E_0)/v} i\,dE}{Q_{Cu,max}} \qquad (13)$$

where $v$ is the potential sweep scan rate ($dE/dt$), $E_0$ is the starting potential of ASV scan, $Q_{Cu,str}$ is the total charge from oxidative stripping of Cu from the time $t_j$ at potential $E_j$ to a final time $t_q$ at potential $E_q$ ; the maximum possible charge, $Q_{Cu,max}$, was determined from the corresponding *ESA* of the pristine $Au_{film}$ described above.

## 3. RESULTS AND DISCUSSION

### *3.1. UPD of Cu on $Au_{film}$*

Figure 3A depicts a typical CV involving the $Cu^{2+}/Cu(s)$ redox process in 0.1 mol/L $HClO_4$ on the $Au_{film}$; characteristically it shows the potential ranges where UPD and overpotential deposition (OPD) of Cu occur in the vicinity of the equilibrium potential ($E_{eq}$) of the $Cu^{2+}/Cu$ redox couple (calculated at about 0.046 V using the Nernst equation taking the bulk concentration of $Cu^{2+}$ ions as 1 x $10^{-3}$ mol/ L). ASV datasets generated from $E_{dep}$ of 0.05 V for $t_{dep}$

between 30 s and 150 s (Figure 3B) exhibited broad doublet stripping peaks consistent with the polycrystalline nature of the $Au_{film}$ substrate used.

From ASV, the *ML*-equivalent trend in the total coverage of Cu on $Au_{film}$ was established as shown in Figure 3C; a reasonably steady total maximum coverage of about 0.8 ML was estimated in this way for $t_{dep}$ between 30 and 150 s. Analysis of potential–coverage ($\theta_{Cu,UPD} - E_{UPD}$) relationship for $Cu_{UPD}/Au_{film}$ system, employing Eqs. (4) - (5), was carried out by multivariate nonlinear curve–fitting for various deposition times, with $E^{\theta\rightarrow 0}$, $f$, $g$, and $z$ as fitting parameters. A representative $Cu_{UPD}$ surface coverage plot (circles) and fitted curves (solid lines) are shown in Figure 3D; the purely Langmuir model of Eq. (4) resulted in inadequate description of the $\theta_{Cu,UPD} - E_{UPD}$ data. From fitting operations using Eq. (5), $E^{\theta\rightarrow 0}$ was systematically found to be in the range 0.330 ± 0.030 V for fitted $\theta_{Cu,UPD} - E_{UPD}$ data sets; remarkably, corresponding to the maximum peak potential of the ASV curves (shown in Figure 3A) where complete electrooxidation of $Cu^0$ adatoms to $Cu^{2+}$ ions is expected to take place. Moreover, in cases when all isotherm fitting parameters were varied, an average $z$ value of about 1.5 (± 0.2) was obtained; a value indicative of an overall two–electron redox process involving Cu adlayer dissolution from the $Au_{film}$ substrate ($Cu^0/Cu^{2+}$ couple).

Moreover, the $f$ parameter, obtained from analysis of $\theta_{Cu,UPD} - E_{UPD}$ with Eq. (5), was found to be rather sensitive to $t_{dep}$. In this regard, for $t_{dep}$ 30 and 60 s the generated $f$ values varied between 1 and 5, whereas for $t_{dep}$ 90 to 150s they varied between –9 and –13. Markedly, regardless of $t_{dep}$, consistent positive $g$ values (in the range 10 – 24) were retrieved. Since the $f$ value, in addition to accounting for substrate-adatom interactions and crystalline heterogeneities, could also be indicative of some variations in the substrate's work function upon Cu UPD and its adlayer

coverage depletion [25, 26]. Hence, longer deposition times (> 90s) might have induced some surface reconfiguration and/or surface alloying between Cu and Au resulting in negative *f* values observed. Since Cu and Au have atomic radii of 0.145 nm and 0.174 nm, respectively, and both metals have cubic–close packed lattice structures, adatom–substrate interactions were expected to be less significant due to the intrinsic heterogeneities of the polycrystalline substrate and the relatively small lattice mismatch between Cu adatoms and Au surface atoms [16, 26, 37, 38].

However, the consistent large positive *g* value, obtained with Eq. (5), was strongly suggestive of prevalent Cu adatom–adatom lateral repulsive interactions. Considerable electronegativity differences between Cu and Au, which in the Pauling scale are 1.9 for the former and 2.4 for the latter [38] plausibly effected some significant charge polarization on the Cu adatoms leading to formation of surface dipoles. In addition, positive values of lateral Frumkin–type interaction parameter involving voltammetric $Cu_{UPD}$ on polycrystalline Pt substrate in acidic medium have also been interpreted to involve Cu–H interactions, in addition to Cu–Cu neighbouring adatoms interactions, where the H–atoms are derived from adsorbed water in the vicinity of the surface active sites of deposition [28].

The contributions of *f* and *g* on the monolayer free energy variation with $Cu_{UPD}$ coverage were clearly observed in plots of $\Delta G_{UPD}$ vs. $\theta_{Cu,UPD}$ from Eq. (6) (results not shown); the $\Delta G_{UPD}$ trend confirmed the spontaneous $Cu_{UPD}$ phase formation where energetics favour the diminishing surface coverage [25, 26].

Having inspected direct $Cu_{UPD}$ monolayer phase formation features on the $Au_{film}$ as a base substrate, it was of great interest and importance to interrogate the trends in the underlying parameters for the $Cu_{UPD}$ adlayer involvement in successive SLRR reactions with $PtCl_6^{2-}$

(employed to generate multilayered Pt). The systematic analysis of kinetics and thermodynamics of these layer-by-layer phase-forming processes is discussed in the following sections.

### *3.2. Physico–chemical analysis of deposition processes of the multilayered $_n(Pt)_{Cu}/Au_{film}$ electrode system*

Figure 4A shows typical potential transients corresponding to various deposition stages as recorded *in situ* during the stepwise formation of the multilayered Pt system $_n(Pt)_{Cu}/Au_{film}$. The potential transients clearly show pre–treatment steps involving rinsing with the background electrolyte (BE) solution (Stage 1) at +0.2 V, phase formation of $Cu_{UPD}$ (Stage 2) at +0.05 V for 90 s, and open–circuit (OC) injection of $PtCl_6^{2-}$ electrolyte solution followed by Pt deposition via SLRR reaction ($SLRR_{Pt}$, Stage 3) where replacement of the $Cu_{UPD}$ with Pt adlayers took place.

Typical CV signatures prior to and after carrying out the multistage deposition are shown in Figure 4B. The disappearance of the Au electrochemical surface feature [32] on the $_n(Pt)_{Cu}/Au_{film}$ electrode system - Au surface oxide reduction peak ***a*** in Figure 4B, as per Reaction (12), was confirmation of successful Pt adlayer coverage on the $Au_{film}$. Moreover, Pt surface electrochemistry [36] is clearly observed on the $_n(Pt)_{Cu}/Au_{film}$ by: (i) recognition of well–pronounced reduction feature of Pt surface oxide layer (peak ***b*** with maximum at 0.4 V), proceeding mainly via Reaction (14), and (ii) typical hydrogen UPD features on polycrystalline Pt, that is, hydrogen adsorption-desorption reaction (Reaction (15)) in the potential range between 0.0 V and –0.2 V (See potential region labelled ***c*** in Figure 4B).

$$Pt(s) + H_2O \leftrightarrow PtO(s) + 2H^+ + 2e^- \quad (14)$$

$$Pt(s) + H^+ + e^- \leftrightarrow Pt\text{–}H_{ads} \quad (15)$$

#### *3.2.1. Modelling adlayer phase formation during $SLRR_{Pt}$*

Having confirmed formation of Pt adlayers on $Au_{film}$, an investigation of the kinetics and thermodynamics during formation of such adlayers involving Reaction (11) for various deposition cycles was undertaken. To this effect, general analytical models of Eqs. (8) – (10) were systematically tested to describe the time-dependent SLRR phase formation through regression analysis performed on $E_{SLRR}$ transients (Stage 3, Figure 4A). In this case, besides the phase formation parameters $f$, $g$, and $E^{\theta\rightarrow 0}$, the phenomenological reaction kinetic parameters ($k_o$, $k_{r1}$, $k_r$ and $N_{or}$) were also optimized for consecutive deposition stages. The overall modelling approach was such that the models were separately tested for $E_{SLRR}$ transients without prior presumption of neither the underlying nature of transport-limitations of ionic species involved nor the reaction order $N_{or}$.

Employing either Eq. (8) or Eq. (9) to fit the appropriate potential transients resulted in non–convergence; this strongly suggests that during respective deposition cycles (i) the diffusion flux of $PtCl_6^{2-}$ ions from the solution phase to the substrate surface was much larger than the rate of SLRR reaction, and (ii) reaction mechanisms with non–zero $N_{or}$ occur [12], regardless of $z$ being set at either 1 or 2 (considering possible stable oxidation states of Cu).

Effectively, the analysis of $E_{SLRR}$ transients was then focused only on the parameters determined by use of Eq. (10) as discussed hereafter; this model yielded best–fit solutions, but only when $z$ was constant at the value of 2 (representative fitted transients are shown in Figure 5). Hypothetical fitted potential curves, where $z$ was set at 1, are also shown as insets in Figure 5; markedly, for all the cycles tested, the scenario of $z$ being unity was implausible. Moreover, modelling results of phase formation of $SLRR_{Pt}$ revealed a distinct decrease in the value of $k_r$ (the phenomenological overall reaction constant in this model) between the first deposition cycle

(which exclusively involved Pt adlayer formation on the Au substrate) and the second deposition cycle involving initial Pt deposition on preformed Pt sites (Figure 6A). Eventually, with further Pt deposition (Cycles ≥ 2), $k_r$ attained a remarkable constancy. Furthermore, the evaluated $N_{or}$ was computed at about 1.8 for the first deposition cycle that took place on bare $Au_{film}$ and decreased to about 1.3 after the third cycle (See Figure 6B).

The trends in $k_r$ and $N_{or}$ for various deposition cycles categorically showed the dissimilarity between the reaction mechanism of Pt phase formation through SLRR on the initial crystalline $Au_{film}$ substrate and gradually formed layered Pt deposits. Indeed, $k_r$ and $N_{or}$ are intricately linked to the fundamental rate constant $k$ of the SLRR reaction and collision frequency between surface $PtCl_6^{2-}$ ions, $Cu_{UPD}$ adatoms, and the activation energy of their activated complexes (intermediate states) during the redox-replacement reaction [12, 39]. Hence, the observed variations in $k_r$ and $N_{or}$ might be understood from the variable activation complexes formed as a result of surface changes induced by the growing Pt nanocluster array-like system on $Au_{film}$. The changing surface properties, charge-polarization, and overall activation energetics of transitional states on the pristine Au|Au surface, mixed substrate involving Au|Pt surface sites, and eventual involvement of layered Pt|Pt interfaces, could have effects on the observed decrease of reaction rate and somewhat involved reaction mechanism of the $SLRR_{Pt}$.

The trend in the fitting $E^{\theta\rightarrow 0}$ (Figure 6C), for the $Cu_{UPD}$ depletion and resultant Pt phase formation through SLRR, is such that it became somewhat more negative with increasing Pt deposition (the initial $E^{\theta\rightarrow 0}$ value of 0.65 V for the first deposition cycle on fresh $Au_{film}$ smoothly decreases throughout the process and approaches a value of ≈ 0.61 V for the final deposition cycle). This decreasing trend could also be attributed to the changing substrate properties, in

particular, the work function of the respective surfaces [25, 26]. The variation in $E^{\theta \rightarrow 0}$ also suggest more favourable energetics, from a thermodynamic point of view, of depletion of $Cu_{UPD}$ adlayer coverage upon redox–replacement with Pt adlayers on $Au_{film}$ in contrast to the $Cu_{UPD}$ coverage diminishment on pre-existing Pt nanocluster array.

Figure 6D exhibits the variations in simultaneously optimized parameters *f* and *g*. Both types of interaction parameters show small variations for the first three cycles or so, and almost constant values of $f = -19\ (\pm 3)$ and $g = 47\ (\pm 3)$ thereafter. The steady values obtained after the third cycle might suggest minimal changes in underlying substrate surface and nature of adatom interactions properties after predominant formation of Pt deposits. In particular, the observed $f < 0$ could be indicative of cumulative effects involving distinctive interactions amongst the adatoms, induced changes in the polycrystalline surface work functions, and overall heterogeneity of the deposition sites [25, 26, 28].

The consistently positive trend in the *g* parameter during consecutive SLRR reactions, from progressively changed Au substrate to Pt layered deposits, might also indicate some interplay of charge polarization effects that led to distinct surface dipoles when Cu adlayers and their subsequent replacement took place solely on Au as compared to their formation and replacement on gradually formed Pt centres (electronegativity value for Cu is 1.9 whereas Pt and Au have values of 2.2 and 2.4, respectively, in the Pauling scale) [38]. The variations in *f* and *g* parameters could also suggest some overcoming of the weak repulsive forces of dipole–dipole nature probably through two–dimensional nucleation and formation of some band structures leading to condensed phase formation [25, 26]. Moreover, the parameters *f* and *g* might also be attributable to characteristic geometric factors, enhancing promotion of nearest adatom-adatom

neighbours within the adlayers as well as two-dimensional coordination of the Cu surface arrays on Pt adlayers as opposed to $Au_{film}$ surface [25, 26].

From above modelling results, essentially generating $z$ as 2, the overall SLRR reaction, in integer stoichiometry, that most likely took place is given by Reaction (16) below

$$2Cu_{UPD}/S + PtCl_6^{2-} \leftrightarrow 2Cu^{2+} + Pt^0/S + 6Cl^- \quad (16)$$

where $S$ is $Au_{film}$ which gradually changed to Pt during formation of the multilayered $_n(Pt)_{Cu}/Au_{film}$ system.

Re–oxidation $Cu_{UPD}$ by $PtCl_6^{2-}$might in principle proceed to $Cu^+$ [11, 12], essentially generating $z$ as 1; perhaps this scenario is plausible only when conditions for significant formation of $CuCl_2^-$ exist or free $Cl^-$ ions availability persist. The nature of the substrate might also have an effect on formation of different activated complexes during redox-replacement, with consequences on observed stoichiometry.

*3.2.2. Gibbs free energy variations during successive SLRR reactions*

The underlying kinetics of phase formation involving SLRR reactions in growth of Pt multilayers through replacement of $Cu_{UPD}$ adlayers, are deductable from models of potential dependency, such as that of Eq. (10), as demonstrated and discussed in the preceding section. Overall thermodynamic driving force and its underlying variation upon such phase formation phenomena can be appreciated from time-dependent Gibbs free energy changes. From $E_{SLRR} - t$ relationship of Eq. (10) and the relationship $\Delta G = zFE$, we phenomenologically introduce the Gibbs free energy change of adlayer formation via SLRR reaction ($\Delta G_{SLRR}$) as function of reaction time $t$ as shown in Eq. (17):

$$\Delta G_{\mathrm{SLRR}} = \Delta G^{\theta\to 0} + RT\left[\ln\left(\frac{\left(1+k_{\mathrm{r}}t\right)^{1/(1-N_{\mathrm{or}})}}{1-\left(1+k_{\mathrm{r}}t\right)^{1/(1-N_{\mathrm{or}})}}\right) + f\left(1+k_{\mathrm{r}}t\right)^{1/(1-N_{\mathrm{or}})} + g\left(1+k_{\mathrm{r}}t\right)^{3/(2-2N_{\mathrm{or}})}\right] \qquad (17)$$

where $R$, $T$, $f$, $g$, $k_{\mathrm{r}}$ and $N_{\mathrm{or}}$ have their usual meaning; $\Delta G^{\theta\to 0} = -zFE^{\theta\to 0}$.

Representative $\Delta G_{\mathrm{SLRR}}$ curves for Reaction (16) at various deposition cycles, as evaluated employing Eq. (17) and using best-fit parameters obtained from regression analysis of $E_{\mathrm{SLRR}}$ - $t$ data sets described above, are plotted in Figure 7. In all cycles, the negatively decreasing $\Delta G_{\mathrm{SLRR}}$ with increasing reaction time is consistent with thermodynamically favoured spontaneous $\mathrm{Cu_{UPD}}$ adatom depletion and concomitant replacement by Pt adatoms. The role of thermodynamics of phase formation involving SLRR reactions performed on an interfacial substrate (that is a substrate composed of two distinct metal adlayers) is clearly discernible from the trend of $\Delta G_{\mathrm{SLRR}}$ as a function of deposition cycles in generation of $_{\mathrm{n}}(\mathrm{Pt})_{\mathrm{Cu}}/\mathrm{Au_{film}}$. Notably, there is an overall positive change in the $\Delta G_{\mathrm{SLRR}}$ as Pt centres are formed away from the base $\mathrm{Au_{film}}$ upon increasing deposition cycles (Figure 7).

Overall, the trends of phenomenological surface coverage parameters during successive SLRR steps as well as variations in $\Delta G_{\mathrm{SLRR}}$ strongly suggest that the $\mathrm{Pt|Au_{film}}$ interface during the first two deposition cycles or so influence the fastest SLRR reaction kinetics and overall favourable thermodynamics as compared to the exclusive replacement of $\mathrm{Cu_{UPD}}$ adlayers proceeding at layered Pt-on-Pt sites which were formed in subsequent deposition stages. The quantitative trends deduced in this work are in agreement with recent qualitative findings from *in situ* scanning tunnelling microscopy of UPD on Au (111) and Pt clusters generated via successive SLRR reactions [14], where a somewhat bimetallic mixed substrate between Au and Pt was suggested to form during initial UPD/SLRR cycles on Au(111) substrate. Moreover, the models

explored here also cement our earlier observations [13] on unique electrocatalytic properties of bimetallic and multilayered nanostructured electrode systems generated via sequential electrodeposition involving SLRR reactions.

## 4. CONCLUSIONS

This work analytically explored applicability of models describing phase formation within the framework of adlayer adsorption–desorption electrochemical isotherms, based on surface coverage variations of underpotentially-deposited adlayers and their involvement in surface–limited redox–replacement reaction. The phase formation processes investigated involved UPD of Cu and sequentially-implemented redox-replacement by $PtCl_6^{2-}$ to form multilayered Pt nanofilm on a crystalline Au film as a base substrate.

Modelling of $Cu_{UPD}$ anodic stripping curves, in the context of combined electrochemical isotherm (of Temkin– and Frumkin–type), successfully described the potential dependency of the monolayer surface coverage of $Cu_{UPD}$ on $Au_{film}$ and its subsequent oxidation to $Cu^{2+}$. Moreover, through multivariate regression analysis, stoichiometric aspects and phenomenological reaction kinetics of the SLRR reaction involving $Cu_{UPD}$ and $PtCl_6^{2-}$ were carried out. The observed curve-fitting solutions compellingly suggested that the SLRR reaction mechanism at various deposition cycles involved re–oxidation of $Cu_{UPD}$ adlayers to $Cu^{2+}$ ions. The SLRR reaction investigated here was derived as second–order with respect to $Cu_{UPD}$ when the reaction took place on pristine Au substrate and markedly fractional in the range 1.3 on subsequent cycles involving Pt centres. The magnitude of the phenomenological SLRR rate constant was found to decrease gradually with multiplication of Pt adlayers, indicative of faster reaction kinetics on bare $Au_{film}$ substrate as opposed to its dispensation on Pt adlayers. The trend in the apparent Gibbs free energy of the

SLRR reaction also exhibited increasing spontaneity with reaction time towards steady–state. The gradual change of substrate effects from predominantly Au to Au|Pt and subsequently Pt|Pt interfacial characteristics also appeared to influence the interplay of adatom interactions, overall reaction kinetics and thermodynamics of phase formation via SLRR reaction. Overall, the physico–chemical model systematically investigated in this work can be useful in design of multilayered systems where successive UPD and SLRR processes form integral parts in their fabrication.

**Acknowledgements**

This work was supported by research funding from University of Pretoria (UP). Special thanks to Dr. Mkhulu K. Mathe (Council for Scientific and Industrial Research, Pretoria, South Africa) and Prof. Dr. John Stickney (Department of Chemistry, The University of Georgia, Athens, USA) for their contribution in acquisition of the gold substrates used in the experimental work. Andre Botha of Microscopy and Microanalysis Unit at UP is thanked for his assistance on FEG–SEM analysis.

**References**

[1] S.R. Brankovic, J.X. Wang, R.R. Adzic, Metal monolayer deposition by replacement of metal adlayers on electrode surfaces, Surf. Sci., 474 (2001) L173.

[2] M.F. Mrozek, Y. Xie, M.J. Weaver, Surface-Enhanced Raman Scattering on Uniform Platinum-Group Overlayers: Preparation by Redox Replacement of Underpotential-Deposited Metals on Gold, Anal. Chem., 73 (2001) 5953.

[3] R. Adzic, Electrocatalysis on Surfaces Modified by Metal Monolayers Deposited at Underpotentials, in: A.J. Bard, M. Stratmann, E. Gileadi, M. Urbakh (Eds.) Encyclopedia of Electrochemistry, vol. 1, WILEY-VCH, Weinheim, 2002, pp. 561.

[4] S. Park, P. Yang, P. Corredor, M.J. Weaver, Transition Metal-Coated Nanoparticle Films: Vibrational Characterization with Surface-Enhanced Raman Scattering, J. Am. Chem. Soc, 124 (2002) 2428

[5] Y.-G. Kim, J.Y. Kim, D. Vairavapandian, J.L. Stickney, Platinum Nanofilm Formation by EC-ALE via Redox Replacement of UPD Copper: Studies Using in-Situ Scanning Tunneling Microscopy, J. Phys. Chem. B, 110 (2006) 17998.

[6] M.B. Vukmirovic, J. Zhang, K. Sasaki, A.U. Nilekar, F. Uribe, M. Mavrikakis, R.R. Adzic, Platinum monolayer electrocatalysts for oxygen reduction, Electrochim. Acta, 52 (2007) 2257.

[7] L.T. Viyannalage, R. Vasilic, N. Dimitrov, Epitaxial Growth of Cu on Au(1110 and Ag(111) by Surface Limited Redox Replacement - An Electrochemical and STM Study, J. Phys. Chem. C, 111 (2007) 4036

[8] Y. Ando, K. Sasaki, R. Adzic, Electrocatalysts for methanol oxidation with ultra low content of Pt and Ru, Electrochem. Commun., 11 (2009) 1135

[9] T.S. Mkwizu, M.K. Mathe, I. Cukrowski, Electrodeposition of multilayered bimetallic nanoclusters of ruthenium and platinum via surface–limited redox–replacement reactions for electrocatalytic applications, Langmuir, 26 (2010) 570.

[10] K. Sasaki, H. Naohara, Y. Cai, Y.M. Choi, P. Liu, M.B. Vukmirovic, J.X. Wang, R.R. Adzic, Core-Protected Platinum Monolayer Shell High-Stability
Electrocatalysts for Fuel-Cell Cathodes, Angew. Chem. Int. Ed., 49 (2010) 8602

[11] D. Gokcen, S.-E. Bae, S.R. Brankovic, Stoichiometry of Pt Submonolayer Deposition via Surface-Limited Redox Replacement Reaction, J. Electrochem. Soc., 157 (2010) D582

[12] D. Gokcen, S.-E. Bae, S.R. Brankovic, Reaction kinetics of metal deposition via surface limited red-ox replacement of underpotentially deposited metal monolayers, Electrochim. Acta, 56 (2011) 5545.

[13] T.S. Mkwizu, M.K. Mathe, I. Cukrowski, Multilayered Nanoclusters of Platinum and Gold: Insights on Electrodeposition Pathways, Electrocatalysis, Surface and Bulk Compositional Properties, J. Electrochem. Soc., 160 (2013) H529

[14] Q. Yuan, A. Tripathi, M. Slavkovic, S.R. Brankovic, Lead Underpotential Deposition on Pt-submonolayer Modified Au(111), Z. Phys. Chem., 226 (2012) 965.

[15] D.M. Kolb, Physical and electrochemical properties of metal monolayers on metallic substrates, in: H. Gerischer, C.W. Tobias (Eds.) Advances in Electrochemistry and Electrochemical Engineering, vol. 11, John Wiley, New York, 1978, pp. 125

[16] E. Herrero, L.J. Buller, H.D. Abruna, Underpotential Deposition at Single Crystal Surfaces of Au, Pt, Ag, and Other Materials, Chem. Rev., 101 (2001) 1897.

[17] N. Dimitrov, R. Vasilic, N. Vasiljevic, A Kinetic Model for Redox Replacement of UPD Layers, Electrochem. Solid-State Lett., 10 (2007) D79.

[18] E.B. Budevski, G.T. Staikov, W.J. Lorenz, Underpotential Deposition of Metals - 2D Phases, in: Electrochemical Phase Formation and Growth: An Introduction to the Initial Stages of Metal Deposition, Wiley-VCH, Weinheim, Germany, 1996, pp. 41

[19] R. Parsons, The thermodynamics of monolayer adsorption in electrochemical systems, J. Electroanal. Chem., 376 (1994) 15.

[20] N. Pangarov, Thermodynamics of Electrochemical Phase Formation and Underpotential Metal Deposition, Electrochim. Acta, 28 (1983) 763.

[21] L. Blum, D.A. Huckaby, M. Legault, Phase Transitions at Electrode Interfaces, Electrochim. Acta, 41 (1996) 2207.

[22] A. Frumkin, O. Petry, B. Damaskin, The Notion of the Electrode Charge and the Lippmann Equation, Electroanal. Chem. Interficial Electrochem., 27 (1970) 81.

[23] V. Sudha, M.V. Sangaranarayanan, Underpotential Deposition of Metals: Structural and Thermodynamic Considerations, J. Phys. Chem. B, 106 (2002) 2699.

[24] K. Engelsmann, W.J. Lorenz, Underpotential Deposition of Lead on Polycrystalline and Single-crystal Gold Surfaces, J. Electroanal. Chem, 114 (1980) 1.

[25] S. Swathirajan, H. Mizota, S. Bruckenstein, Thermodynamic Properties of Monolayers of Silver and Lead Deposited on Polycrystalline Gold in the Underpotential Region, J. Phys. Chem., 86 (1982) 2480.

[26] S. Swathirajan, S. Bruckenstein, Thermodynamics and Kinetics of Underpotential Deposition of Metal Monolayers on Polycrystalline Substrates, Electrochim. Acta, 28 (1983) 865

[27] B.E. Conway, H. Angerstein-Kozlowska, Interaction Effects in Electrodeposited Monolayers and the Role of the Electrosorption Valency Factor, J. Electroanal. Chem, 113 (1980) 63.

[28] L.H. Mascaro, S.A.S. Machado, L.A. Avaca, Determination of lateral interaction parameters for copper monolayers on polycrystalline platinum, J. Chem. Soc., Faraday Trans., 93 (1997) 2577.

[29] E. Kirowa-Eisner, Y. Bonfil, D. Tzur, E. Gileadi, Thermodynamics and kinetics of upd of lead on polycrystalline silver and gold, J. Electroanal. Chem., 552 (2003) 171

[30] C. Thambidurai, Y. Kim, J.L. Stickney, Electrodeposition of Ru by atomic layer deposition (ALD), Electrochim. Acta, 53 (2008) 6157.

[31] S. Bourkane, C. Gabrielle, F. Huet, M. Keddam, Investigation of Gold Oxidation in Sulfuric Medium - I. Electrochemical Impedance Techniques, Electrochim. Acta, 38 (1993) 1023

[32] L.D. Burke, P.F. Nugent, The Electrochemistry of Gold: 1 The Redox Behaviour of the Metal in Aqueous Media, Gold Bulletin, 30 (1997) 43.

[33] S.B. Brummer, A.C. Makrides, Surface Oxidation of Gold Electrodes, J. Electrochem. Soc., 111 (1964) 1122

[34] P.S. Germain, W.G. Pell, B.E. Conway, Evaluation and origins of the difference between double-layer capacitance behaviour at Au-metal and oxidized Au surfaces, Electrochim. Acta, 49 (2004) 1775

[35] S. Trasatti, O.A. Petrii, Real Surface Area Measurements in Electrochemistry, J. Electroanal. Chem., 327 (1992) 353.

[36] A. Bard, L.R. Faulkner, Electrochemical methods: Fundamentals and Applications, 2nd ed., John-Wiley & Sons, New York, 2001.

[37] S. Ye, K. Uosaki, Atomically Controlled Electrochemical Deposition and Dissolution of Noble Metals, in: A.J. Bard, M. Stratman (Eds.) Encyclopedia of Electrochemistry, vol. 1, Wiley-VCH, Weinheim, 2002, pp. 471.

[38] D.R. Lide, CRC Handbook of Chemistry and Physics, in, Taylor and Francis, Boca Raton, FL, 2005.

[39] P.L. Houston, Chemical Kinetics and Reaction Dynamics, McGraw-Hill, New York, 2001.

## FIGURE CAPTIONS

**Figure 1.** (A) Flow–cell assembly for electrochemical deposition on a gold thin–film substrate. (B) – (C) Schemes showing the sequential electrodeposition routes to form monometallic Pt multilayers on $Au_{film}$ substrate via surface–limited redox–replacement reactions involving UPD of Cu.

**Figure 2.** (A) FEG–SEM micrograph showing the morphology of a typical bare $Au_{film}$ substrate. (B) XRD pattern of $Au_{film}$. (C) Representative CVs recorded on $Au_{film}$ in 0.1 mol/L $HClO_4$ at indicated scan rates, showing Au surface oxide features (peak ***a***) – see text for details.

**Figure 3.** (A) Representative CVs recorded on $Au_{film}$ at a scan rate of 5 mV/s in 1 x $10^{-3}$ mol/L $Cu^{2+}$ in 0.1 mol/L $HClO_4$ solution showing UPD and OPD of Cu; the inset is a CV recorded in narrower potential range. In all CVs the initial scanning was carried out in the direction indicated by the broken arrow. (B) ASV curves after UPD of Cu at +0.05 V for the indicated deposition time. (C) Trend in the total coverage in monolayer–equivalents for the $Cu_{UPD}/Au_{film}$ system derived from ASV for the applicable deposition time. (D) Representative electrochemical isotherm for $Cu_{UPD}/Au_{film}$ obtained from analysis of ASV after deposition at 0.05 V for the indicated $t_{dep}$; circles are experimentally-derived data and solid lines are fitted curves based on the indicated model isotherms.

**Figure 4.** (A) Potential transients recorded *in situ* during multistage deposition of the multilayered Pt electrode system $_n(Pt)_{Cu}/Au_{film}$ via SLRR reaction involving $Cu_{UPD}$ and $PtCl_6^{2-}$ ($SLRR_{Pt}$). 0.1 M $HClO_4$ was the background electrolyte used for preconditioning and rinsing purposes between UPD of Cu and $SLRR_{Pt}$; Cyc = deposition cycle. (B) CVs of bare $Au_{film}$ and

$_n(Pt)_{Cu}/Au_{film}$ after eight deposition cycles recorded in 0.1 M $HClO_4$ at scan rate of 50 mV/s. The initial scanning direction is indicated by broken arrows.

**Figure 5.** Representative potential transients for various deposition cycles during multilayer Pt deposition on $Au_{film}$ involving $Cu_{UPD}$ redox–replacement by Pt ($SLRR_{Pt}$). Circles are experimental data and solid lines are best–fit curves using the analytical model of Eq. (10) where $E^{\theta\rightarrow 0}$, $f$, $g$, $k_r$, and $N_{or}$ were simultaneously optimized whilst z was kept constant at a value of 2. *Insets*: hypothetical curves (dotted lines), computed with $z$ kept constant at a value of 1.

**Figure 6.** Trends of the parameters (A) $k_r$, (B) $N_{or}$, (C) $E^{\theta\rightarrow 0}$, and (D) variations in interaction parameters $f$ and $g$ obtained from modelling with Eq. (10) for various deposition cycles during electrochemical generation of the multilayered electrode system $_n(Pt)_{Cu}/Au_{film}$.

**Figure 7.** Gibbs free energy variations of the SLRR reaction (Reaction 16) computed using Eq. (17) at various deposition cycles to generate $_n(Pt)_{Cu}/Au_{film}$.

**Figure 1**

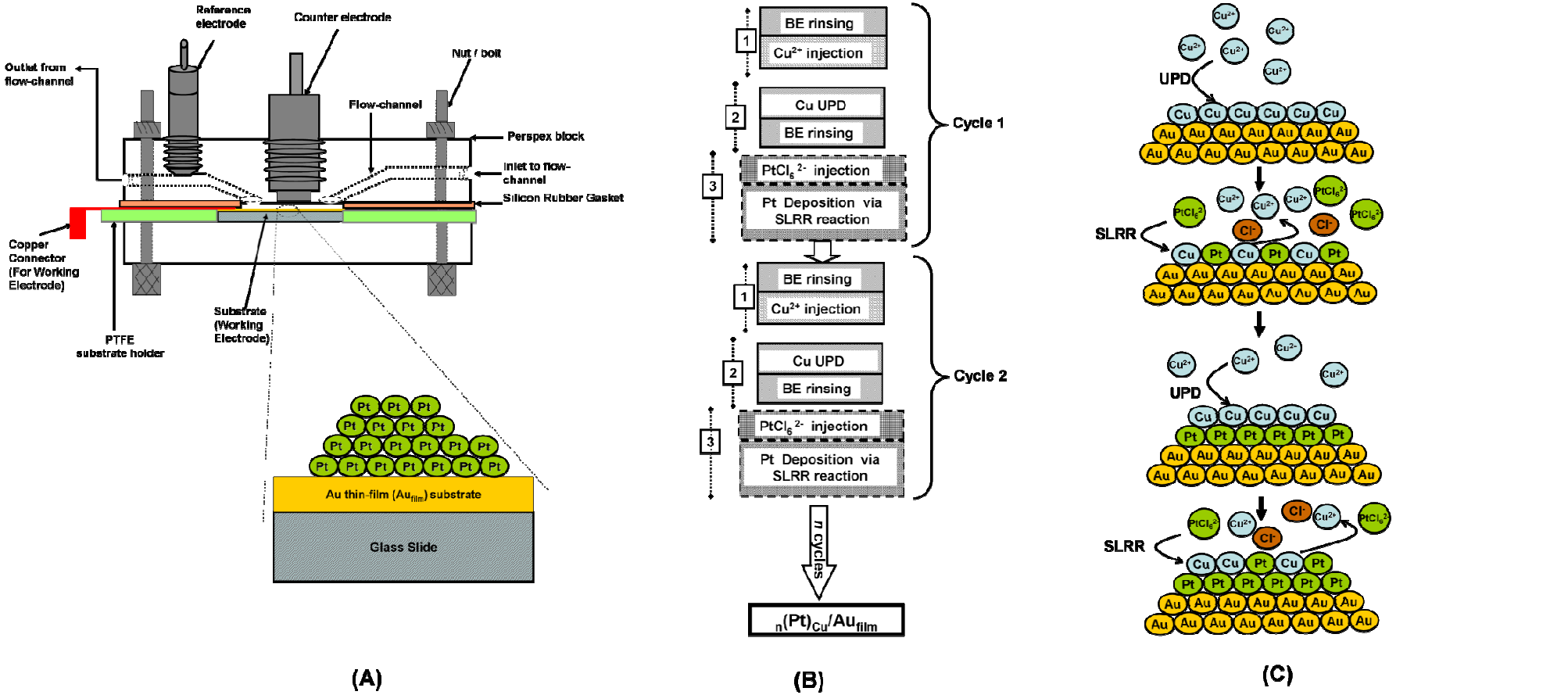
Reference electrode
Counter electrode
Nut / bolt
Outlet from flow-channel
Flow-channel
Perspex block
Inlet to flow-channel
Silicon Rubber Gasket
Copper Connector (For Working Electrode)
PTFE substrate holder
Substrate (Working Electrode)
Au thin-film (Au$_{film}$) substrate
Glass Slide
(A)
1
BE rinsing
Cu$^{2+}$ injection
2
Cu UPD
BE rinsing
3
PtCl$_6^{2-}$ injection
Pt Deposition via SLRR reaction
Cycle 1
1
BE rinsing
Cu$^{2+}$ injection
2
Cu UPD
BE rinsing
3
PtCl$_6^{2-}$ injection
Pt Deposition via SLRR reaction
Cycle 2
n cycles
$_n$(Pt)$_{Cu}$/Au$_{film}$
(B)
UPD
SLRR
UPD
SLRR
(C)

**Figure 2**

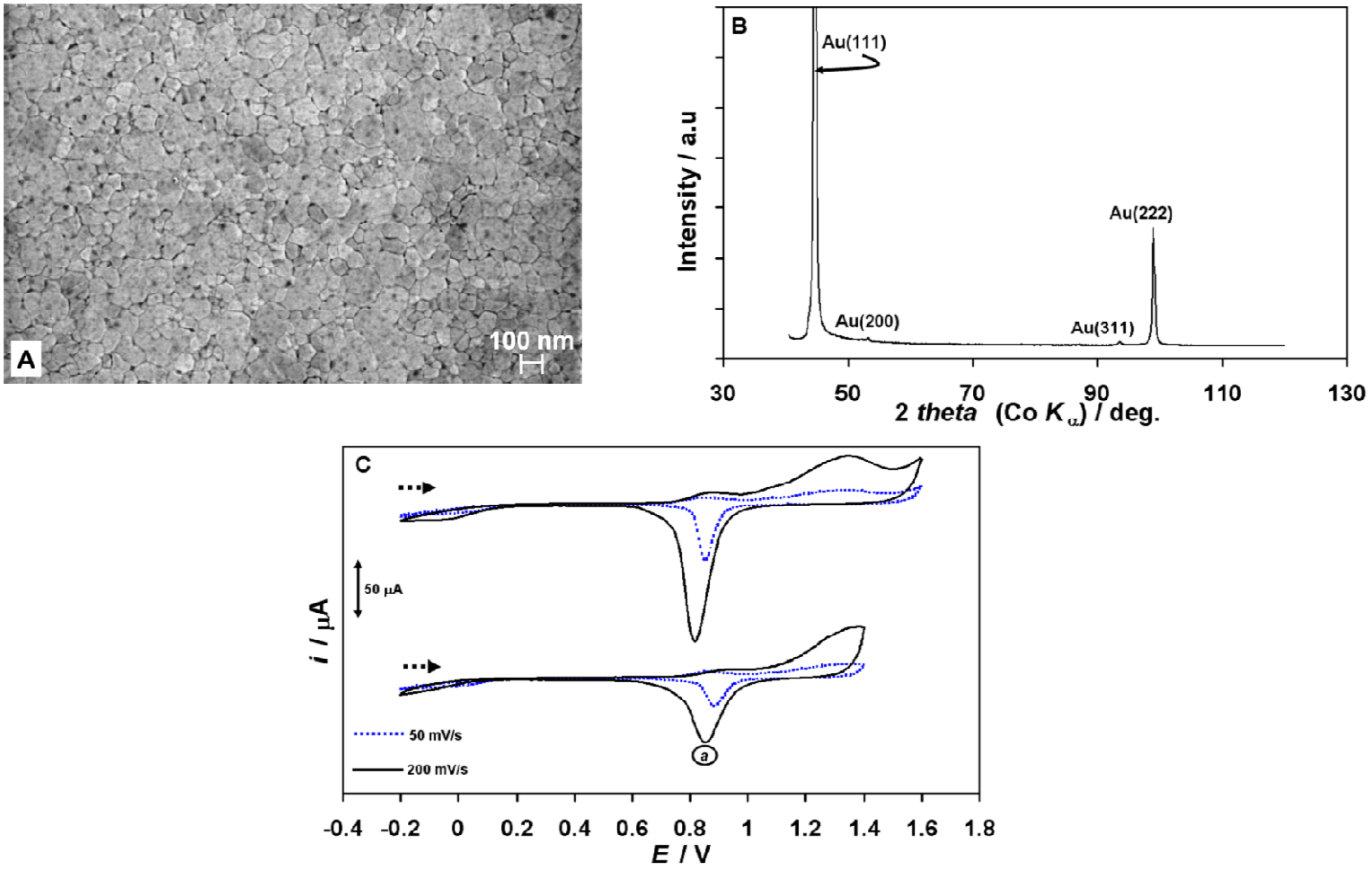
A
100 nm
B
Au(111)
Au(222)
Au(200)
Au(311)
Intensity / a.u
30
50
70
90
110
130
2 theta (Co K$_\alpha$) / deg.
C
50 µA
i / µA
50 mV/s
200 mV/s
a
-0.4
-0.2
0
0.2
0.4
0.6
0.8
1
1.2
1.4
1.6
1.8
E / V

**Figure 3**

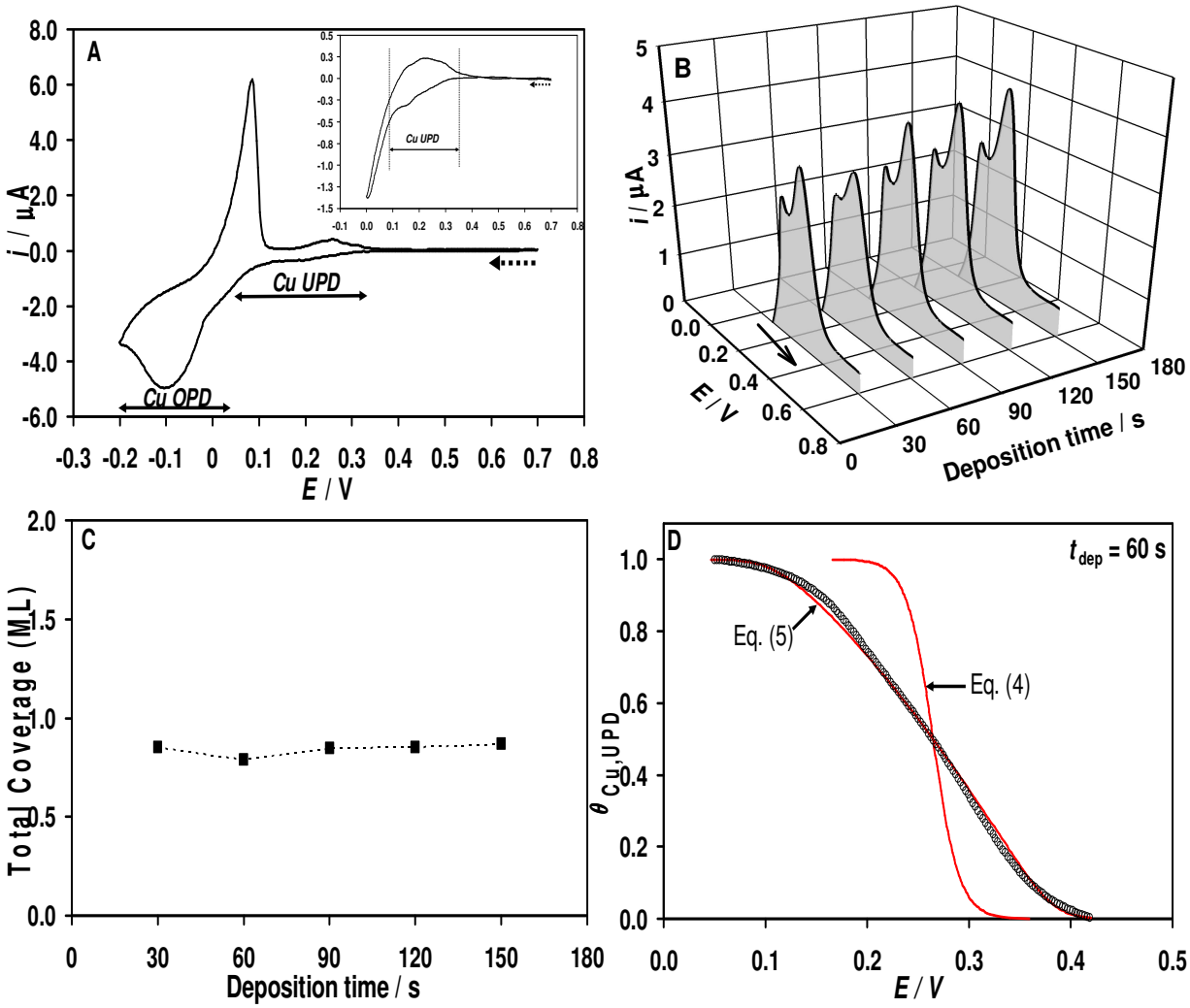
A
Cu UPD
Cu OPD
i / μA
E / V
B
i / μA
E / V
Deposition time / s
C
Total Coverage (ML)
Deposition time / s
D
t dep = 60 s
Eq. (5)
Eq. (4)
θ Cu,UPD
E / V

**Figure 4**

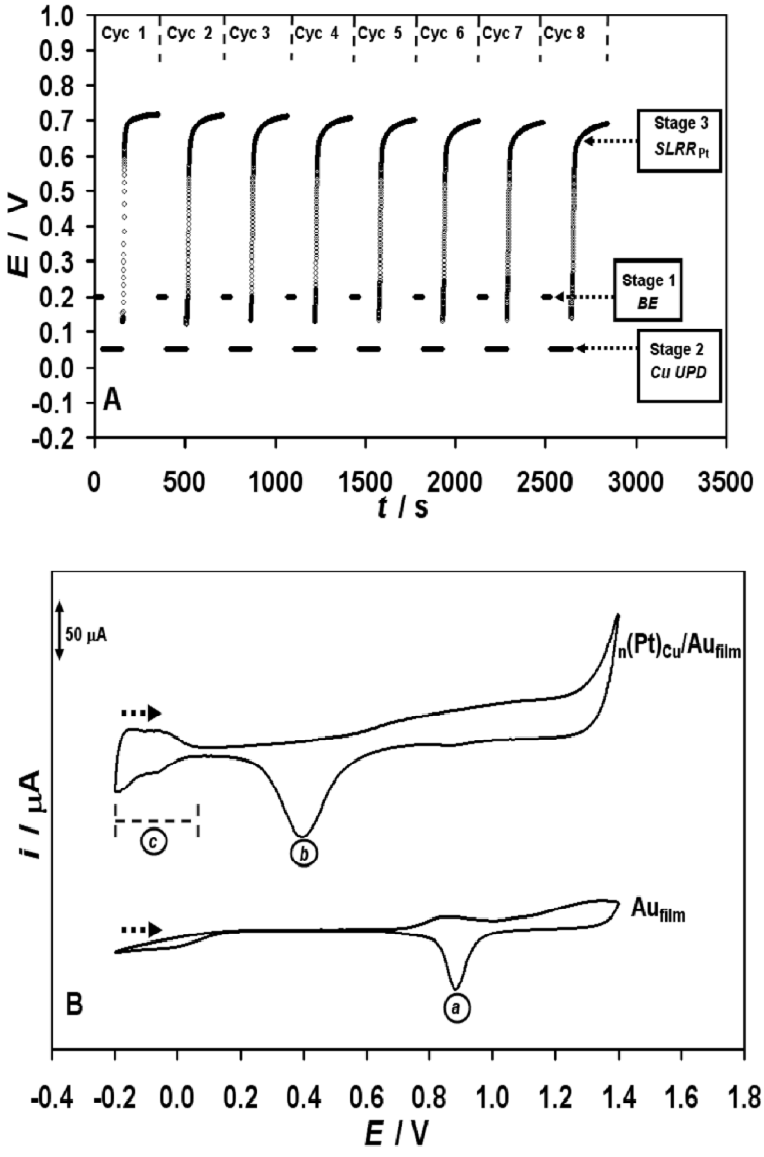
Cyc 1
Cyc 2
Cyc 3
Cyc 4
Cyc 5
Cyc 6
Cyc 7
Cyc 8
Stage 3
SLRR Pt
Stage 1
BE
Stage 2
Cu UPD
A
E / V
t / s
50 μA
n(Pt)Cu/Aufilm
Aufilm
c
b
a
B
i / μA
E / V

**Figure 5**

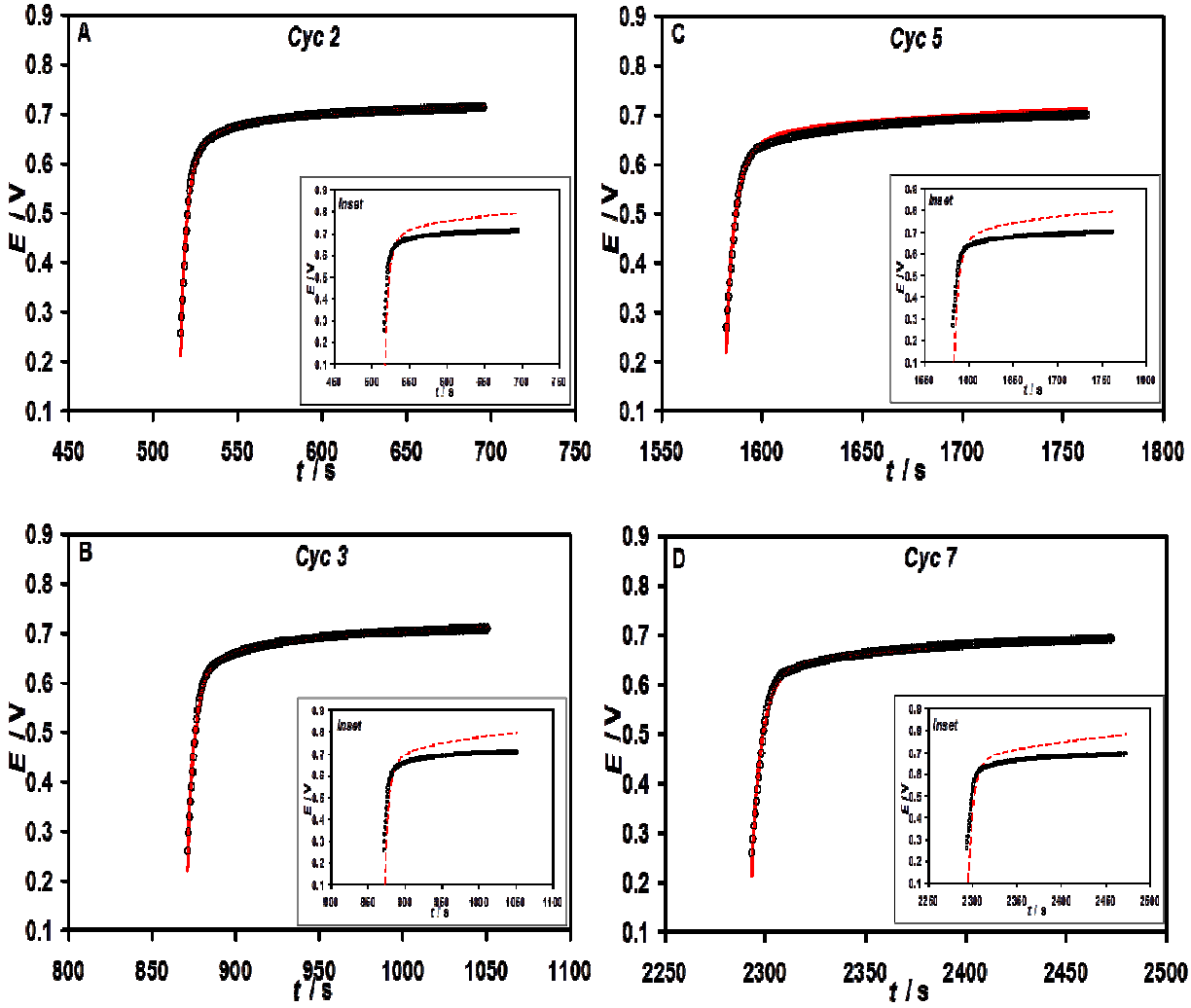

**Figure 6**

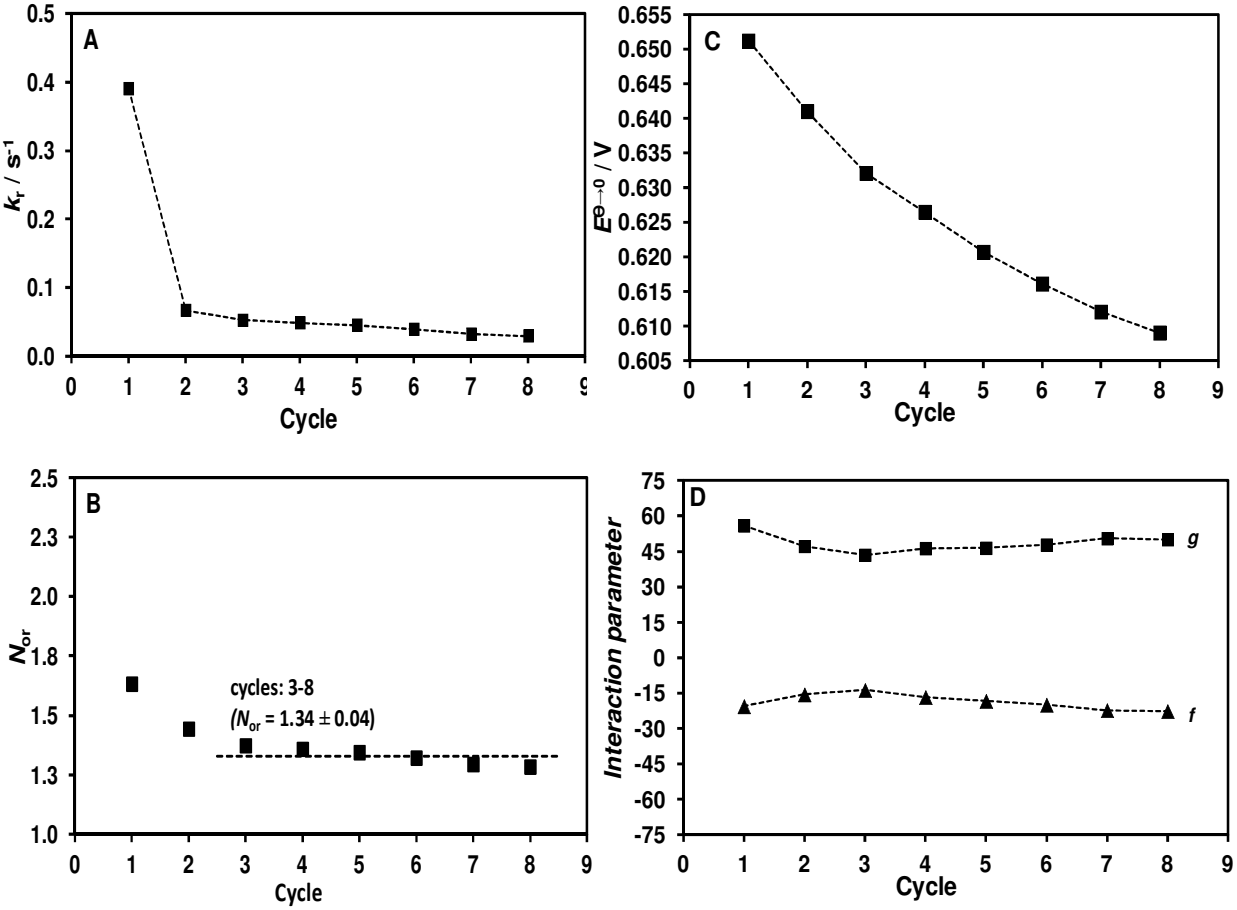
A
$k_r$ / s$^{-1}$
Cycle
C
$E^{\ominus\rightarrow 0}$ / V
Cycle
B
$N_{or}$
cycles: 3-8
($N_{or}$ = 1.34 ± 0.04)
Cycle
D
Interaction parameter
g
f
Cycle

**Figure 7**

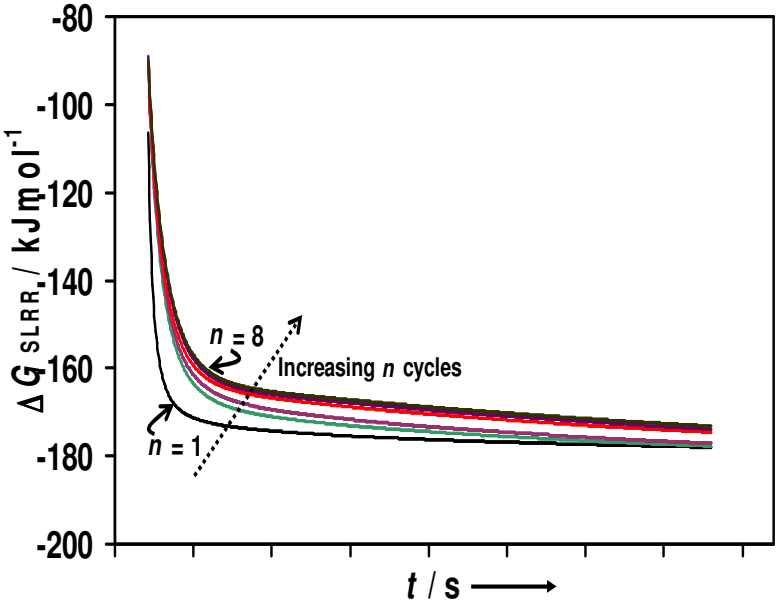
-80
-100
-120
-140
-160
-180
-200
ΔG SLRR / kJmol-1
n = 8
Increasing n cycles
n = 1
t / s